Co-delivery of RNAi and chemokine by polyarginine nanocapsules enables the modulation of myeloid-derived suppressor cells

Adriana M. Ledo[a], Maria S. Sasso[b,c], Vincenzo Bronte[d], Ilaria Marigo[b], Ben J. Boyd[e],
Marcos Garcia-Fuentes[a], María J. Alonso[a,*]

[a] Department of Pharmacology, Pharmacy and Pharmaceutical Technology, CIMUS Research Institute, Universidade de Santiago de Compostela, 15782 Santiago de Compostela, Spain
[b] Veneto Institute of Oncology IOV-IRCCS, 35128 Padova, Italy
[c] Institute for Molecular Engineering, The University of Chicago, Chicago, IL, USA
[d] Department of Medicine, Verona University Hospital, 37134 Verona, Italy
[e] ARC Centre of Excellence in Convergent Bio-Nano Science and Technology, and Drug Delivery, Disposition and Dynamics, Monash Institute of Pharmaceutical Sciences, Monash University, Parkville Campus, 381 Royal Parade, Parkville, VIC 3052, Australia

ABSTRACT

Myeloid-Derived Suppressor Cells (MDSCs), immunosuppressive cells that promote tumor growth, represent an attractive target in cancer immunotherapy. However, the clinical success of this strategy is limited by the lack of efficient drug delivery vehicles targeting this cell compartment. The objective of this work was to develop a delivery carrier, multilayer polymer nanocapsules, with the capacity to co-encapsulate two types of immunomodulatory drugs, a chemokine and an RNAi sequence, aimed at reverting MDSC-mediated immunosuppression. The chemokine CCL2, intended to attract monocyte-macrophage MDSCs, was encapsulated within the L2 inverse micellar aqueous domains of the lipid core of these nanocapsules. On the other hand, two different RNAi sequences that modulate the CCAAT/enhancer-binding protein beta (C/EBPβ) pathway, shC/EBPβ and miR 142-3p, were successfully associated to their polymer shell. These RNAi sequences were covered by subsequent layers of polyarginine and hyaluronic acid, thereby creating multi-layered assemblies that protected them and facilitated their targeted delivery. The in vitro studies performed in primary MDSCs cultures showed the capacity of miR 142-3p-loaded nanocapsules to reduce the highly immunosuppressive monocyte-macrophage subset. Additionally, the encapsulation of CCL2 within the nanocapsules induced a potent monocyte-macrophage chemoattraction that could be used to direct the therapy to these cell subsets. Finally, in vitro and in vivo studies showed the capacity of shC/EBPβ-loaded nanocapsules to downregulate C/EBPβ levels in MDSCs and to reduce monocyte differentiation into tumor-associated macrophages in an MCA-203 fibrosarcoma mice model. In conclusion, the multilayer polymer nanocapsules described here are efficient vehicles for the co-delivery of proteins and RNA, and are potential candidates as nanomedicines for the modulation of MDSCs.

1. Introduction

Myeloid-derived suppressor cells (MDSCs), immature myeloid cells that impair T cell activity [1], represent a promising target to increase the efficacy of cancer immunotherapies, especially in the case of adoptive T cell transfer (ACT) [2–4]. Several molecular and biochemical hallmarks are associated with MDSCs and could be used as pharmacological targets to prevent their generation or modulate their function. In order to impair tumor-induced MDSC accumulation, CCAAT/enhancer-binding protein beta (C/EBPβ) transcription factor (TF) holds a special interest since it forms a feedback loop with miR-

142-3p promoting myeloid cell differentiation towards immunosuppressive macrophages [5]. Bearing this in mind, some authors have shown that both, the silencing of C/EBPβ and miR-142-3p over-expression, using poly(amidoamine) (PAMAM) dendrimers as carriers, leads to a reversion of the tumor-induced tolerance and, hence, to a therapeutic benefit in tumor-bearing mice [6]. However, despite these promising results, this is to the best of our knowledge the only work exploring RNAi-based therapies to target the C/EBPβ pathway in MDSCs.

Chemokine targeting is another valuable therapeutic strategy to modulate the tumor immune infiltrate and enhance the immune-

mediated rejection of cancer [7]. In particular, the targeting of chemokine CCL2, secreted by the majority of solid cancers, has been extensively investigated [8–12]. The CCL2-CCR2 axis is implicated in the migration of MDSCs to the tumor [13], with a preferential effect on the monocyte subset [8,14,15], and this MDSCs accumulation hampers cytotoxic T cells (CTLs) recruitment, thus limiting the efficacy of cancer immunotherapy [16,17]. Moreover, CCL2 is nitrated/nitrosylated by reactive nitrogen species produced by the tumor impeding its ability to attract tumor-specific CTLs, but maintaining its capability to recruit MDSCs, further promoting the mechanism of tumor escape [16,18,19]. Although the majority of chemokine targeting strategies have been intended to block their signaling cascades [20], new pharmaceutical approaches have also tried to boost chemotactic circuits in order to attract host immune cells to cancer vaccination devices, and to help direct adaptive immune responses [21–23].

Despite the contribution of nanotechnology to the development of new cancer treatments [24], and the recent advances in cancer immunotherapies, the use of delivery carriers targeting the MDSC compartment is still in its infancy. Of note, the majority of such nanotechnological approaches rely on poorly defined semi-synthetic immunogenic structures [25–29] or aim to evaluate the effect of classical chemotherapeutic agents on the MDSC subset [30–32]. More sophisticated strategies have been explored to target tumor-associated macrophages (TAMs) [33], however, compared to the unequivocal tumor-promoting activity of MDSCs, TAMs can exert either tumor-promoting or anti-tumor effects [34]. For this reason, there is a need for new, rationally-designed, nanocarriers targeting MDSCs. Trying to address this problem, in the present study, we develop multilayer polymer nanocapsules (NCs) specifically designed to co-deliver two immunomodulatory drugs: RNAi polynucleotides with the capacity to modulate the C/EBPβ pathway and the chemokine CCL2, which was meant to attract monocyte-macrophage MDSCs and T cells. In particular, we have investigated two RNAi strategies involving the use of either miR 142-3p or C/EBPβ-targeted shRNA, both capable of reducing C/EBPβ-mediated MDSCs generation. Among the chemokine repertoire, CCL2 was chosen due to its potent chemoattractant activity on monocyte-macrophage cells, which led us to hypothesize that the release of CCL2 from the nanosystems could attract this specific MDSCs subset to the NCs. The subsequent NCs uptake was expected to lead to the intracellular delivery of RNAi molecules on these target cells. MDSC targeting is also supposed to be promoted by the natural tropism of the nanosystems for the tumor [35] and spleen [36], which are sites of major MDSC accumulation [37,38]. Additionally, CCL2 release within the tumor site may also contribute to locally attract CTLs, which are also responsive to this chemokine, further supporting immune-mediated tumor destruction.

In order to achieve the association of both RNAs and CCL2 to the NCs, we took advantage of the RNA condensing capacity of the polyarginine shell, and we created a glyceryl-monooleate (GMO)-based liquid-crystal core where the chemokine can be encapsulated within its aqueous domains [39,40]. In addition, polyarginine was chosen based on its transcytotic and endosomal scape abilities [41] that have been successfully employed by our research group to facilitate intracellular drug delivery [42–46]. These RNA-loaded NCs were provided with additional polyarginine and hyaluronic acid polymer layers in order to protect the RNA cargo and facilitate targeting. The NCs were extensively characterized in terms of their physicochemical properties and structural organization, as well as with regard to their macrophage chemoattractant capacity and ability to downregulate C/EBPβ splenic and tumor levels in a mouse model of fibrosarcoma. Overall, this work describes the development and assessment of a new immunomodulatory nanovehicle capable of both, attracting myeloid cells and promoting the reversion of their immunosuppressive phenotype by modulating the C/EBPβ pathway.

2. Materials and methods

2.1. Preparation of ovalbumin and CCL2-loaded nanocapsules

Preparation of GMO NEs consisted on the preformation of a GMO cubic phase gel loaded with OVA, which was subsequently mixed with Labrasol® and dispersed in a Pluronic® F127 aqueous solution. To prepare the GMO cubic gel, 5 mg of GMO (Danisco) were melted at 37–40 °C and mixed with 1.67 μL of warm water (blank NEs) or the same volume of a warm solution containing 125 μg OVA (InvivoGen) (OVA-loaded NEs). The mixture was vortexed (30 s, 2000 rpm) and equilibrated for 2 days at room temperature to yield 6.7 mg of the cubic phase gel. After the equilibration process, 45 μL of Labrasol® (Gattefossé) (1:9 GMO:Labrasol w:w ratio) were mixed with the gel by vortexing (30 s, 2000 rpm) and the aqueous solution containing 5.75 mg of Pluronic® F127 (Sigma) was subsequently added. NEs were magnetically stirred for 30 min at 300 rpm and stored at 4 °C until further use.

Polyarginine nanocapsules (NCs) were prepared by the adsorption of polyarginine onto pre-formed GMO NEs. Specifically, 2.2 mL (5.75 mg) of the Pluronic® F127 solution were poured onto the lipid phase under magnetic stirring (5 min, 300 rpm), then 250 μL of poly-L-arginine hydrochloride (MW 5–15 KDa, Sigma) solution (5 mg/mL) were added to a final volume of NCs (2.5 mL). For the preparation of CCL2-loaded NCs, several GMO cubic phase gels were prepared, as previously described, that contained either 0.625, 1.25 or 2.5 μg of murine CCL2 (Peprotech) to yield 0.25, 0.5, and 1 μg/mL CCL2-loaded NCs, respectively. Both the NEs and NCs were isolated by ultracentrifugation (1 h, 25,000 rpm and 15 °C) in an Ultracentrifuge Beckman Coulter ProteomeLab™ XL-A/XL-I to determine the encapsulation efficiency of the protein payloads. All NCs were prepared in ultrapurified water (Milli-Q Plus water purification system, Millipore).

2.2. Preparation of RNA-loaded polyarginine nanocapsules

RNA-loaded NCs were prepared by incubating purified polyarginine NCs with a RNA solution (2 μg/μL) (IDT), at a theoretical polyarginine:RNA ratio of 1:1 or 2:1 (w/w), i.e. 24.7 mg/mL of NCs were loaded with 0.4 or 0.2 mg/mL of RNA. After the association, the formulation was immediately vortexed for 30 s and left 20 min for stabilization at room temperature. RNA-loaded NCs at a 1:1 (w/w) ratio were, then, incubated with another layer of polyarginine, or with a double layer of polyarginine and hyaluronic acid so as to obtain: coated 1:1:1 pArg:RNA:pArg NCs or double-coated 1:1:1:6 pArg:RNA:pArg:HA NCs. NCs were lyophilized before storage. For the preparation of the polyarginine-coated system, 0.2 volumes of a polyarginine solution (2 μg/μL) were added onto 1 volume of RNA-loaded polyarginine NCs, immediately mixed by vortex (30 s, 2000 rpm), and incubated 20 min at room temperature. An extra layer of sodium hyaluronate (MW 40 KDa, Lifecore) could be added by mixing polyarginine-coated NCs with a hyaluronic acid solution (10 μg/μL) following the same protocol. Particles that incorporated both active components, chemokine and RNA, were prepared by incubating CCL2-loaded NCs with the RNA solution. All RNA-loaded NCs were prepared in RNase free water (Life Technologies).

2.3. Physicochemical and morphological characterization of the nanocapsules

Particle mean size and polidispersity index (PDI) were determined by dynamic light scattering (DLS), and zeta potential was calculated from the eletrophoretic mobility values obtained by laser Doppler anemometry in a Nanosizer ZS® (Malvern Instruments) equipped with a red laser light beam (λ = 632.8 nm). Measurements were made at 25 °C with a 1/100 (v/v) sample dilution in ultrapure water. The results shown are the mean of 3 successive measurements of at least 3

independent samples. For the evaluation of the colloidal stability of the NCs in different biorelevant media, NCs were diluted 1/10 (v/v) in the corresponding medium, incubated for the desired time and further diluted 1/10 (v/v) in ultrapure water before DLS measurements were performed. Sample morphology was assessed by transmission electron microscopy (JEOL JEM-1011). NCs were stained with osmium tetroxide, vacuum dried, and placed on cupper grids before observation.

2.4. Determination of OVA encapsulation efficiency

The encapsulation efficiency of ovalbumin in the NEs was analyzed by UPLC. UPLC analysis was conducted on an Acquity H-class system equipped with an Acquity UPLC Peptide BEH300 C18 1.7 μm, 2.1 × 50 mm column. Samples were analyzed using 0.1% trifluoroacetic acid (TFA) in water (Mobile Phase A) and 0.08% TFA in acetonitrile (Mobile Phase B) with the following gradient: 0 min-2% B, 1 min-70% B, 2 min-73.2% B, 4 min-73.2% B, 6 min-80% B, 7 min-2% B, 8 min-2% B. The flow rate was 0.2 mL/min and the column temperature was 60 °C. Injection volume was 5 μL and detection was conducted at 214 nm. Nanoemulsions with a theoretical amount of 50 μg/mL were prepared and isolated by ultracentrifugation as previously described. The resultant supernatants and isolated fractions were diluted with 0.08% TFA acetonitrile before injection. OVA concentration was calculated based on calibration curves made in diluted supernatants and isolated fractions of blank particles. The encapsulation efficiency percentage (EE%) was referred as a mass ratio of the amount of OVA in the isolated fractions to the total amount of OVA in the complete sample.

2.5. Determination of CCL2 encapsulation efficiency

The encapsulation of CCL2 within the lipidic core of the particles was determined by a sandwich ELISA. Encapsulation efficiency was evaluated in the nanoemulsions due to the high interference of polyarginine in epitope recognition when NCs were assayed. Nanoemulsions with a theoretical amount of 0.25 μg/mL CCL2 were prepared and isolated by ultracentrifugation. Supernatants were diluted with PBS and the CCL2 concentration was calculated by extrapolation from a calibration curve drawn using diluent (0.05% (w/v) Tween® 20, 0.1% (w/v) BSA in PBS). The total amount of CCL2 was calculated by extracting CCL2 from samples of NCs with Triton™ X-100 before isolation. In this case, CCL2 concentration was calculated by extrapolation from a calibration curve drawn using diluent supplemented with 0.08% (w/v) Triton™ X-100, the final amount of Triton™ X-100 in extracted samples. CCL2 was detected with a secondary antibody conjugated with horseradish peroxidase (HRP), and the quantification was done spectrophotometrically, after incubation (10 min, 37 °C) with HRP substrate 2,2′-azino-di-(3-ethylbenzthiazoline sulfonic acid) (ABTS). Absorbance readings were performed at 405 nm, with wavelenght correction at 650 nm, in a Multiskan FC microplate photometer (Thermo Fisher Scientific). Supernatants and total samples of blank nanoemulsions were used as blanks to subtract nonspecific background signals. Percentage encapsulation efficiency was calculated as previously described.

The loading of CCL2 was calculated by dividing the total amount of encapsulated CCL2 by the total weight of the NCs. The total weight of NCs was obtained by calculating the weight of the NCs after their isolation, which represents the yield of NC formation. For this, 2 mL of NCs were isolated by ultracentrifugation and 500 μL of reconstituted isolated NCs, and 250 μL of non-isolated NCs were lyophilized in previously weighted 1.5 mL tubes. Tubes were weighted after lyophilization, and the yield of NC formation was obtained by dividing the mass of isolated by the mass of non-isolated NCs.

2.6. Evaluation of RNA association and integrity

For the qualitative determination of the efficiency of the RNA association to the surface of the NCs, samples were loaded in agarose (2% w/v in Tris Acetate-EDTA buffer) or polyacrylamide gels (15% w/v in Tris Borate-EDTA buffer) before and after the incubation with an excess of heparin for RNA displacement. Each gel lane was loaded with the same amount of RNA (from 0.4 to 1 μg), either adsorbed to the NCs or displaced from their surface with heparin in order to determine both the adsorption efficiency and the integrity of the RNA. For heparin displacement, heparin was added (25:1 w:w heparin:RNA) and samples were incubated for 30 min at 37 °C and 300 rpm (Incubator 1000, Heidolph). Control lanes (RNA only) were included to check for smeared bands. Gels were run for 1 h at 90 and 120 V, in a Sub -Cell GT cell 96/192 (Bio-Rad, Hercules, CA, USA) for agarose and polyacrylamide gels, respectively. Loading buffer contained 0.1% w/v glycerol, and 1× SYBR®Gold nucleic acid stain (Life Technologies) for sample visualization. Gels were imaged with a Molecular Imager® Gel Doc™ XR System (Bio-Rad). A quantification of RNA association efficiency was performed by determining the concentration of RNA in the supernatant of NCs after centrifugation (20,817 RCF, 1 h, Centrifuge 5430R, Eppendorf). Supernatants were measured in a Nanodrop® 2000 UV–Vis Spectrophotometer (Thermo Fisher Scientific) using the supernatant of blank NCs as blank. Adsorption efficiency (AE%) was then calculated based on the theoretical loading of miRNA.

2.7. In vitro release of OVA and RNA

OVA release was determined upon the incubation of the NEs in PBS at 1/10 dilution under horizontal shaking (Incubator 1000, Heidolph). NEs were isolated by ultracentrifugation, and the concentrated isolated fraction was diluted in PBS pH 7.4 and incubated for 0, 4, and 6 h at 37 °C and 300 rpm. Samples were then ultracentrifuged and supernatants were collected for UPLC analysis. RNA release assays after incubation of NCs in full human plasma, PBS, or complete culture medium (DMEM 10% FBS, 100 U/mL penicillin, and 100 μg/mL streptomycin) were performed with displacement assays using polyacrylamide gels. NCs were incubated with the media at various dilutions (1/10, 1/50, 1/100) for 4, 8, and 12 h at 37 °C, and 300 rpm under horizontal shaking. At the desired time points, samples were retrieved and a volume of diluted NCs and diluted NCs incubated with heparin corresponding to a total amount of 400–800 ng RNA were loaded in 15% polyacrylamide gels. Gel displacement assays were performed as described in Section 2.6 with the exception of samples incubated in plasma. In this last case, heparin incubation was performed during 30 min on ice, spinning the samples for 30 s in a vortex mixer every 5 min, to avoid RNA degradation. For the same reason, electrophoresis was also performed on ice. In addition, samples were diluted at least 1/2.5 for gel loading to avoid plasma autofluorescence.

2.8. SAXS sample preparation and analysis

Bulk GMO phases were prepared with increasing GMO content. GMO was weighed into glass HPLC vials and heated at 40 °C until it melted, when the appropriate amount of water was added. Mixtures were immediately vortexed and allowed to equilibrate for ≥48 h. GMO-Labrasol® mixtures with increasing Labrasol® content were also prepared. GMO gel was weighed into glass vials and mixed with Labrasol® by a vortex mixer. Finally, NCs and nanoemulsions were prepared as previously described (Section 2.2). Bulk samples were transferred to a stainless-steel paste cell (approx. 2 mm diameter, 1 mm sample thickness) and sealed with Kapton tape on both sides, while dispersed nanocapsule systems were transferred to quartz capillaries (1.5 mm diameter, Charles Supper) after their isolation by centrifugation. Capillaries were then inserted into a thermostatted metal heating block controlled by a waterbath to 37 ± 0.1 °C. Sample temperature

was established by a thermocouple inserted into a spare sample position in the holder. Measurements were performed on the SAXS/WAXS beamLine at the Australian Synchrotron [47]. An X-ray beam with a wavelength of 0.83 Å (11 keV) was selected. The 2D SAXS patterns were collected using a Pilatus 1 M detector (170 mm × 170 mm) located 900 mm from the sample position. The total q range for the instrument configuration outlined above was $0.02 < q < 1.06°A^{-1}$. 2D SAXS patterns were collected for 1 s, and the computer software Scatterbrain was used to acquire and reduce the 2D patterns to 1D intensity vs. q profiles. Phase structures were identified by indexing Bragg peaks to known relative spacing ratios and lattice dimensions, a, were calculated using known relationships described by Hyde [48]. Calibration was done against silver behenate.

2.9. Migration assay in RAW 264.7 macrophages

Macrophage migration in response to encapsulated CCL2 was analyzed by a transwell assay using 24 well inserts (6.5 mm) with 8 μm pore size polycarbonate membranes (Corning). RAW264.7 cells were grown in DMEM high glucose with L-glutamine supplemented with 10% v/v fetal bovine serum (FBS), 100 U/mL penicillin and 100 μg/mL streptomycin (Life Technologies). Cells were maintained at 37 °C in a humidified incubator supplied with 5% CO_2, and split by scrapping at 80% confluency. Macrophages were starved for 12 h by culturing them in migration buffer (DMEM supplemented with 1% FBS, 100 U/mL penicillin and 100 μg/mL streptomycin). Then, 0.5×10^6 cells in 100 μL of migration buffer were added to the upper chamber of the insert. The lower chamber contained 600 μL with either blank or CCL2-loaded NCs. NCs were prepared as previously described, concentrated 2 times after ultracentrifugation, and mixed with 3× migration buffer and PBS to reach a dose of 100 ng CCL2 in the basal compartment. Blank NCs were mixed in the same proportions and used as controls. After 12 h of migration at 37 °C in a 5% CO_2 atmosphere, cells in the upper chamber that had not migrated were carefully removed with cotton swabs. Migrated cells were then fixed in paraformaldehyde and stained with DAPI. RAW264.7 cells found on the membrane facing the lower chamber were counted as cells having performed chemotaxis, and mean fluorescence intensity (MFI) was quantified with ImageJ software [49]. Ten random fields at 10× magnification were used for cell counting and fluorescence quantification. Mean values and standard deviation were calculated for each independent experiment.

2.10. Transfection and differentiation assays in MDSCs

Primary MDSCs were generated in vitro as previously described [50] and incubated for 4 days at 37 °C with 5% CO_2. MSC1 cells, an immortalized MDSC cell line [51], were grown in RPMI 1640 supplemented with L-Glutamine, Na-Pyruvate and 10% FBS (Life Technologies). For transfection experiments, MDSCs and MSC1 cells were plated in 24 well-plates (50,000 cells/well) 24 h before transfection with 0.1 nmol of miRNA and 15 pmol of shRNA per well. Naked sequences were complexed with GeneSilencer® (Genlantis) or Lipofectamine® RNAiMAX (Invitrogen) following manufacturer's instructions, to be used as positive controls. The day of transfection, medium was replaced with RPMI without antibiotics (Lipofectamine® RNAiMAX, NCs) or without antibiotics and serum (GeneSilencer®), and complexes were mixed with RPMI and added to the cells. Lyophilized NCs were reconstituted in a small amount of RNase free water (3–4 μL), mixed with RPMI and added to the cells. Cells were analyzed 24 h later. MDSCs from the non-adherent and adherent fraction were collected by rinsing the plates with PBS 2 mM EDTA, and phenotypic markers were evaluated by flow cytometry. Silencing of C/EBPβ in MSC1 was quantified by qRT-PCR.

2.11. Cytofluorimetric analysis

MDSCs were washed with cold PBS and incubated 10 min at 4 °C with purified anti-FcγR antibody (clone 2.4G2) to minimize non-specific antibody binding. Antibodies of interest were added to cell suspensions following FcγR blocking and incubated 20 min at 4 °C in the dark. The antibodies used in the study were: anti-CD11b PE-Cy7 (clone M1/70), anti-CD11b PerCP-Cy5.5 (clone M1/70), anti-Ly6G APC-Cy7 (clone 1A8), and anti-Ly6C eFluor 450 (clone HK1.4) (all from eBioscience). Aqua LIVE/DEAD® dye (Invitrogen) was used to analyze cell viability. Flow data were acquired with the help of a BD LSRII or BD FACS Calibur instrument and analyzed with FlowJo (Tree Star, Inc.) software.

2.12. RNA extraction and qRT-PCR

TRIzol® reagent (Invitrogen) was added directly to the culture plate after medium removal, and total RNA was extracted according to the TRIzol® extraction protocol. Following TRIzol® extraction, genomic DNA contaminants were removed using the TURBO DNA-free™ Kit (Ambion). cDNA was generated using the reverse transcriptase SuperScript II and polydT12–18 primers (Invitrogen). PCR and fluorescence detection were performed using the ABI 7900HT fast real-time PCR Systems in a reaction volume of 20 μL containing 1× TaqMan® Universal PCR Master Mix (Applied Biosystems) and 50 ng cDNA. For quantification of mouse Cebpb and Rn18s the 1× TaqMan® Gene Expression Assays Mm00843434_s1 and Mm03928990_g1 (Applied Biosystems) were used. All measurements were performed in duplicates and data were analyzed by the ΔΔCt relative quantification method. Gene expression levels were normalized to the respective endogenous control (Rn18s), and compared with the reference samples.

2.13. Mice

C57BL/6 (WT), were purchased from Charles River Laboratories (Italy) and maintained under specific pathogen-free conditions in the animal facilities of the Istituto Oncologico Veneto (Padova, Italy). Female mice 8–12 weeks old were chosen for these experiments. Experiments involving animals were performed according to the national guidelines and approved by the local ethics committee.

2.14. In vivo treatments on tumor bearing mice

MCA-203 (haplotype H-2b) fibrosarcoma cells were obtained from the American Type Culture Collection and cultured in DMEM 10% FBS (Gibco) supplemented with 2 mM L-glutamine, 10 mM HEPES, 20 μM 2β-Mercaptoethanol, 150 U/mL streptomycin, 200 U/mL penicillin. To establish tumors, MCA203 cells (1×10^6 cells/mouse) were injected subcutaneously on the left flank of C57BL/6 mice, and tumor growth was monitored every 2 days by digital calipers. Intravenous injections of shRNA-loaded polyarginine NCs were started at day 11 from MCA203 tumor cell injection, when tumor surfaces were approximately 35 mm², and repeated 3 times with 48 h intervals (RNA dose = 20 μg/mouse/treatment).

2.15. Statistical analysis

The statistical analysis was performed using GraphPad Prism. Where applicable, data are reported as the mean ± SD. Data were compared using either the unpaired two-tailed Student's *t*-test or one-way ANOVA, and *p*-values ≤.05 were considered to be statistically significant.

3. Results

3.1. Development of GMO-Polyarginine nanocapsules for the co-association of proteins and polynucleotides

3.1.1. Development of the core nanoemulsion that enables the encapsulation of proteins

A critical goal of this work was to design a nanocarrier that could co-allocate two different molecules, a protein (CCL2) and a polynucleotide (C/EBPβ-targeted shRNA or miR 142-3p). To this end, we designed oily nanocores, specially adapted to encapsulate proteins, enveloped by a polymer shell with the capacity to associate polynucleotides. Hence, the first step was the formation of the oily core for which we identified glyceryl monooleate-based mesophases as promising structures for protein encapsulation [39] [40]. Glyceryl monooleate (GMO) is an amphiphilic lipid capable of forming various crystalline phases upon dilution with water [52]. These phases are usually dispersed by highly energetic procedures to yield nanoparticles, subsequently stabilized by the surfactant Pluronic® F127 [53,54]. Given that these procedures may represent a risk for the encapsulated payload [55], in this work we studied the use of the self-emulsifying compound Labrasol® as a co-surfactant to promote a mild mesophase dispersion.

Based on the GMO-water phase diagram, a cubic phase gel suitable for protein encapsulation can be obtained at physiological temperature and pressure [56]. Accordingly, this cubic gel was selected as a bulk material for the core composition (75% GMO + 25% water) and its liquid crystalline structure was confirmed by small angle X-ray scattering (SAXS). In agreement with previous literature [52], the GMO gel showed a cubic structure with a lattice parameter that changed from an "Ia3d" to a "Pn3m" phase upon hydration (Fig. S1A, Supporting information). However, the addition of Labrasol® to promote the nanodispersion of the GMO gel could alter its cubic phase, therefore, the phase distribution of the GMO-Labrasol-water ternary system at 37 °C was investigated. The results shown in Fig. 1A indicate that the cubic phase was maintained when the amount of Labrasol® incorporated to the GMO gel was below 10% (90% GMO in excess water). At 20% Labrasol®/80% GMO, the crystalline structure changed from an inverse bicontinuous cubic phase of the double diamond (Pn3m) space group, to an inverse hexagonal phase coexisting with an L2 inverse micellar phase and, above that quantity, it shifted entirely to an L2 inverse micellar phase. These L2 inverse micellar phases, together with bicontinuous hexagonal phases, are particularly adequate for achieving controlled protein release profiles [54]. Hence, the co-surfactant Labrasol® was selected to investigate its capability to disperse the bulk GMO gel, yielding GMO-based nanocarriers suitable for protein encapsulation.

A formulation method based on these crystal phase changes was first tested with the model protein ovalbumin (OVA) [56]. For this method, a GMO cubic phase gel loaded with OVA was formed first, and subsequently mixed with Labrasol® and dispersed in the Pluronic® F127 aqueous solution (Fig. 1B, Fig. S2, Supporting Information). Different GMO:Labrasol® w:w ratios (i.e. 1:0.5, 1:2, 1:4, 1:9) at a fixed GMO:-Pluronic® F127 w:w ratio (1:1.15) were evaluated in terms of particle size and polydispersity index to generate GMO-based nanoemulsions. Based on this initial screening, a GMO:Labrasol® ratio of 1:9 was selected as the oily cores, yielding monodisperse nanoemulsions with a size and zeta potential of approximately 200 nm and − 20 mV, respectively (Fig. 1C; Table S1, Supporting Information).

The resulting GMO-based nanoemulsions were subsequently coated with a polyarginine shell to elaborate the nanocapsules (NCs), and both, polyarginine NCs and the control nanoemulsions (NEs), were analyzed by SAXS. The characteristic wave of the L2 phase at ≈ 0.15 A^{-1} was observed in both systems (Fig. 1D), thus confirming the suitability of the formulation method to obtain L2 phases for protein encapsulation. Indeed, GMO-based NEs showed encapsulation efficiencies of OVA of 35% as assessed by UPLC, and these NEs retained the majority of the

protein (60%) upon high dilution in phosphate buffer saline. SAXS analysis of the raw materials confirmed that the L2 phase corresponds to a particular NE/NC structure arrangement and is not an inherent property of the materials used (Fig. S1B, Supporting Information).

3.1.2. Design and development of single layer RNAi and CCL2-loaded polyarginine nanocapsules

Once we defined the composition of the NEs to be used as a template for the formation of the polymer shell (Fig. 2A), we analyzed the assembly of one or multiple polymer layers and the co-encapsulation of the chemokine CCL2 and two different types of RNA interference (RNAi) sequences: miRNA (miR) and shRNA (shR). In a first step, CCL2 was encapsulated within the GMO-water gel and polyarginine NCs were produced following the experimental conditions defined for the formation of the NEs (Experimental section), by adding polyarginine into the external aqueous phase. Three nominal CCL2 concentrations, 0.25, 0.5, and 1 μg/mL, were tested, resulting in sizes and surface charges of 150 nm and + 40 mV, respectively, similar to those of blank (non-loaded) NCs (Fig. 2B, C). CCL2 encapsulation within the nanoemulsions was also adequate, showing 50% efficiency as assessed by ELISA (Fig. 3B).

Next, NCs were loaded with increasing amounts of RNA and characterized according to their physicochemical properties. Two RNA:polyarginine w:w ratios, 2:1 and 1:1, were tested during this initial screening, both resulting in NCs with adequate physicochemical properties (Fig. 2B, C, D) and RNA association efficiencies. The association of RNA to polyarginine NCs was first assessed qualitatively by gel retardation assays. NCs with miRNA and shRNA payloads were loaded onto electrophoresis gels before and after their incubation with an excess of heparin. This highly negatively charged polymer competes with the RNA for adsorption to the particles cationic surface and promotes its displacement. As observed in Fig. 3A, the RNA bands are only visible after the addition of heparin, suggesting a tight association of the RNA molecules to the NCs surface. Importantly, CCL2-loaded NCs were able to efficiently adsorb the RNAi sequences, demonstrating the potential of polyarginine NCs for the *co*-allocation of proteins and polynucleotides. In the case of miRNA-loaded systems, encapsulation efficiency was quantified by a Nanodrop® spectrophotometer after centrifuging the nanoparticles and measuring the resultant supernatant to detect the unbound RNA. The results in Fig. 3B indicate that the association efficiency obtained by this method was 70%, further supporting the results obtained by the gel retardation assays.

3.1.3. Assembly of multiple-layer HA-polyarginine-RNA-polyarginine nanocapsules

Based on their RNA encapsulation efficiency and colloidal properties, polyarginine NCs with the highest RNA loading (1:1 ratio) were selected for in vitro experiments aimed at generating single and multiple-layer NCs with improved RNA protection (Fig. 2A). To this end, RNA-loaded polyarginine NCs were coated with an additional layer of polyarginine or a double layer of polyarginine-hyaluronic acid. Of the several polymer weight ratios explored, 1:1:1 and 1:1:1:6 pArg:RNA:-pArg and pArg:RNA:pArg:HA w:w ratios generated the NCs with the best colloidal properties (Fig. 2B, C). Size, polydispersity index (PDI) and surface charge of these multi-enveloped NCs were evaluated by dynamic light scattering (DLS) and laser doppler electrophoretic mobility, respectively. DLS measurements indicated that both blank and RNA-loaded particles had an average hydrodynamic diameter between 150 and 200 nm and a PDI close to 0.1. The zeta potential oscillated from positive to negative values depending on the charge of the polymeric coating (Fig. 2B, C, Table S1). Examination of the NCs using transmission electron microscopy (TEM) revealed particles within the range predicted by DLS measurements. As shown in Fig. 2D, blank NCs exhibited a size of around 200 nm and a spherical shape while miRNA-loaded NCs presented a bigger and sharper shape. The larger size of the loaded particles, together with their more electron dense surface,
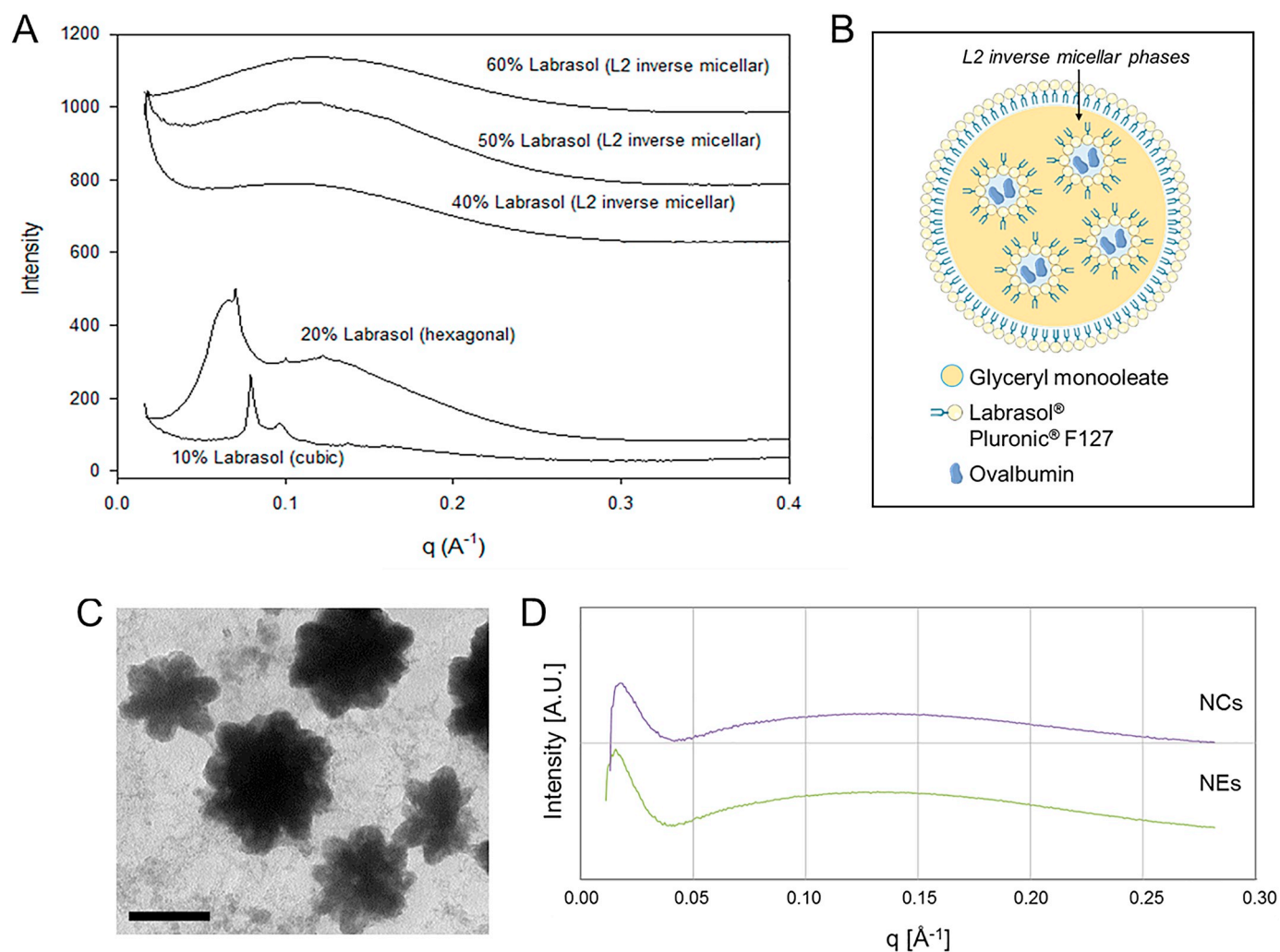
Fig. 1. Physicochemical characterization of NEs as NCs core compositions. A) SAXS profiles showing crystalline phase changes in the GMO precursor gel, while in excess water, with increasing Labrasol® content. B) Scheme illustrating the structure of GMO-based NEs. C) TEM image of OVA-loaded NEs. Scale bar = 200 nm. D) SAXS of polyarginine NCs and the corresponding NEs. SAXS profiles are offset in intensity for clarity.

provide an indication of their effective adsorption of RNA. The morphology of miRNA-loaded NCs was slightly altered in the presence of the polymeric coatings, as shown by the presence of electron dense particles with more spherical shapes.

3.2. Stability and release profile of CCL2 and RNAi-loaded nanocapsules upon storage and incubation in bio-relevant media

3.2.1. Stability of CCL2 and RNAi-loaded nanocapsules upon freeze-drying

The stability of the nanoparticles in dried powder form is a basic prerequisite from a pharmaceutical development standpoint. Consequently, RNA-loaded NCs were freeze-dried and their particle size and RNA association and integrity analyzed after resuspension. Powder NCs were stored for different periods of time at −20 °C, and then resuspended and loaded onto electrophoresis gels before and after incubation with heparin. RNA bands were only observed after the incubation with heparin, indicating that storage time did not induce release of the payload (Fig. 3D). Moreover, displaced RNA bands and the control bands had a similar appearance, which indicates the integrity of the cargo even after 1-year storage (Fig. 3D). Finally, the results obtained by DLS after NCs powder resuspension revealed the same size and polydispersity index than the freshly prepared NCs, thus confirming the colloidal stability of the systems (Fig. 3C).

3.2.2. Study of the stability of RNAi associated with the nanocapsules and assessment of their release in plasma

The release and stability of the RNA upon incubation of RNAi-loaded NCs in plasma were investigated by gel retardation assays. miRNA-loaded NCs were incubated in human plasma for 4 h with a 1/10 dilution (theoretical concentration of NCs and RNAi, 2 mg/mL and 40 μg/mL, respectively). After 4 h, aliquots of the media were loaded in 15% polyacrylamide gels before and after incubation with heparin. As observed in Fig. 4, RNA bands were only detected after incubation with heparin, suggesting that there was no RNA release during the incubation period. However, the fact that the bands were faint indicates that miRNA molecules were partially degraded even though they remained associated to the NCs (Fig. 4A, Fig. S3). Two alternative approaches were tested to circumvent this problem: the use of RNase resistant shRNA sequences and the envelopment of the NCs with single and multiple polymer layers (Fig. 2). The use of RNase resistant sequences confirmed the absence of release from the polyarginine NCs and the maintenance of shRNA integrity (Fig. 4B). The coating of the NCs with polyarginine and polyarginine-hyaluronic acid protected the labile miRNA sequence they carried from its degradation and prevented its release (Fig. 4C, D). Further release studies performed in different biorelevant media also showed the absence of free miRNA (Fig. S4 and Fig. S5, Supporting Information), highlighting the adequate release profile of these NCs. Colloidal stability in these media was confirmed by
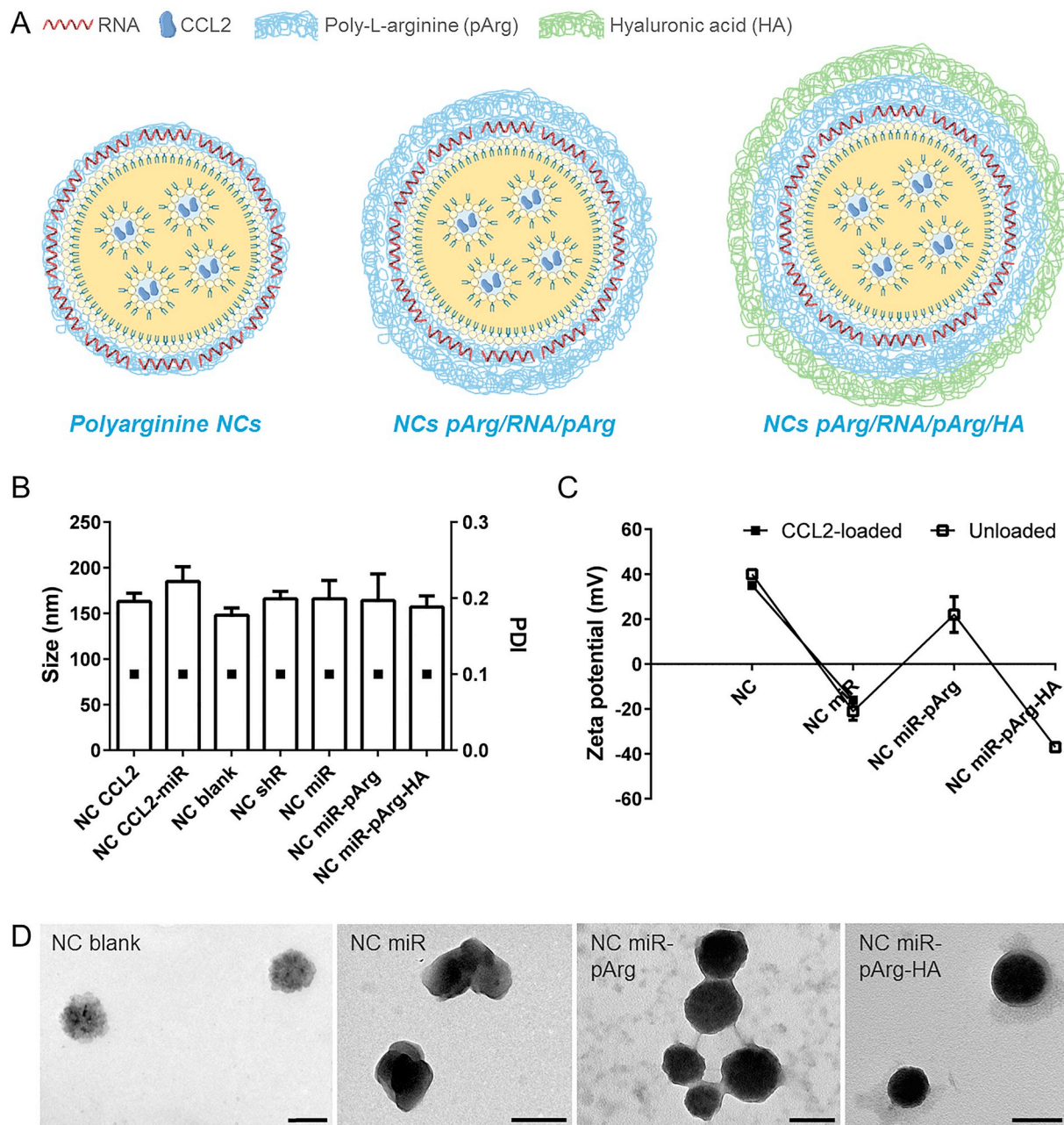
Fig. 2. Characterization of polyarginine NCs. A) Schematic representation of single and multiple layer polyarginine NCs. B) Size and PDI of blank and loaded polyarginine NCs as measured by DLS. C) Zeta potential values of blank and loaded polyarginine NCs. D) TEM micrographs of blank and miRNA-loaded NCs after resuspension from a freeze-dried powder. All scale bars = 200 nm.

DLS measurements (Fig. S6–8, Supporting Information).

3.3. In vitro and in vivo evaluation of the performance of CCL2 and miRNA-loaded polymer nanocapsules

3.3.1. Bioactivity of CCL2-loaded nanocapsules by macrophage migration assay

Transwell migration assays with RAW264.7 macrophages were performed to test the bioactivity of the encapsulated CCL2. RAW264.7 macrophages were seeded on top of the Transwell membranes, and treatments were added in the wells underneath. Cell migration towards CCL2 was evaluated based on the amount of cells that crossed the membrane. Given that polyarginine is a known TLR4 activator [57], and that TLR4 activation stimulates macrophage migration [58], blank NCs were first tested to evaluate basal macrophage migration. Indeed,

treatment with increasing concentrations of blank particles was found to induce macrophage migration in a dose-dependent manner (Fig. 5A). Based on these results, polyarginine NCs with a CCL2 concentration of 1 μg/mL were selected for the migration assays. Considering CCL2 loading, encapsulation efficiency and NCs production yield, a dose of 100 ng CCL2 corresponds to 3 mg NCs. This NCs dose resulted in a minimum basal migration derived from the nanocarrier itself (Fig. 5B). Under these conditions, CCL2-loaded NCs induced significantly higher cell migration compared to blank NCs, suggesting the potential of CCL2-loaded NCs for monocyte-macrophage targeting (Fig. 5C).

In addition, a T cell invasion assay towards CCL2 was performed to mimic the process of cytotoxic T cell (CTL) recruitment to the tumor. To this end, Matrigels® of 10 mg/mL were loaded with soluble CCL2 (60 ng per 100 μL gel), or maintained as such (blank gels) and allowed to gel at 37 °C in a cell incubator. T cells were then added on top of the gels and
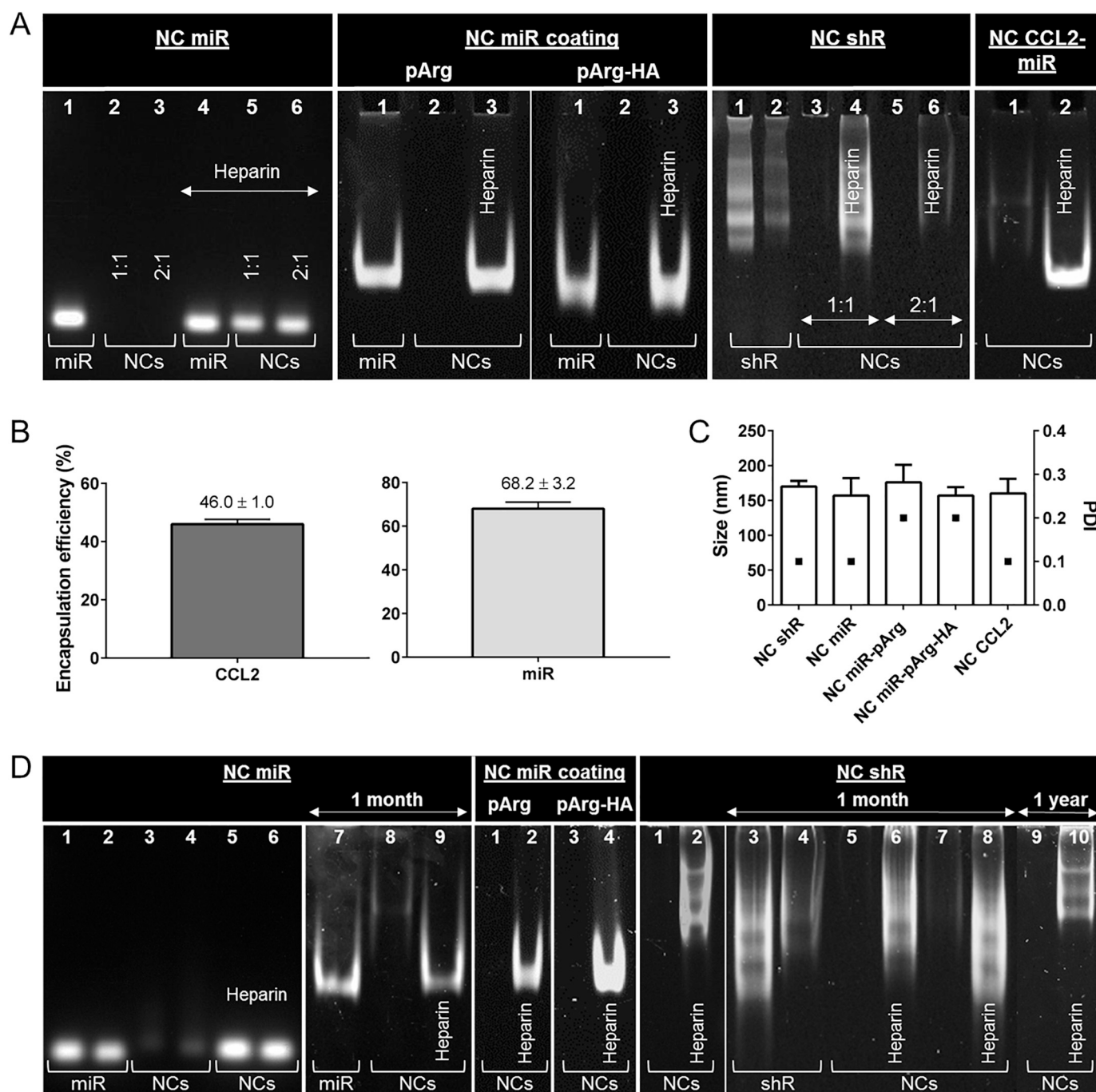
Fig. 3. Physicochemical properties and encapsulation efficiency of fresh and freeze-dried RNA and CCL2-loaded NCs. A) RNA association assay by gel electrophoresis. NC miR lanes: (1) miR control sequence in solution, (2) and (3) NCs with 1:1 and 2:1 polyarginine:miR w:w ratios, (4) miR control incubated with heparin, (5) and (6) NCs 1:1 and 2:1 incubated with heparin. NC miR coating lanes: (1) miR control sequence in solution, (2) Coated NCs, (3) Coated NCs incubated with heparin. NC shR lanes: (1) and (2) 800 and 400 ng shR in solution, (3) and (5) NCs 1:1 and 2:1 polyarginine:shR (800 and 400 ng shR), (4) and (6) NCs 1:1 and 2:1 incubated with heparin. NC CCL2-miR lanes: (1) NCs CCL2-miR, (2) NC CCL2-miR incubated with heparin. B) Encapsulation and association efficiency of CCL2 and miR in NCs as assessed by UPLC and spectrophotometry, respectively. Values represent the mean ± SD ($n = 3$). C) Particle size and PDI of freeze-dried NCs after resuspension. Values represent the mean ± SD (n = 3). D) RNA stability after reconstitution of fresh, 1 month- and 1 year-stored freeze-dried NCs. NC miR lanes: (1) and (2) miR control and miR 142-3p in solution, (3) and (4) NCs miR control and NCs miR 142-3p, (5) and (6) NCs miR control and NC miR 142-3p incubated with heparin (7) miR control, (8) NCs miR control, (9) NCs miR control incubated with heparin. NC miR coating lanes: (1) and (3) pArg coated NCs and pArg- HA coated NCs, (2) and (4) pArg coated NCs and pArg- HA coated NCs incubated with heparin. NC shR lanes: (1) NCs shR control, (2) NCs shR control incubated with heparin, (3) and (4) shRNA control and shCEBP/β sequences in solution, (5) and (7) NCs shR control and NCs shCEBP/β, (6) and (8) NCs shR control and NCs shCEBP/β incubated with heparin, (9) NCs shR control, (10) NCs shR control incubated with heparin.

incubated for 48 h, after which gels were washed and the cells that remained associated to the gels were stained and imaged. As observed in Fig. S13, CCL2-matrigels promoted a higher T cell invasion, suggesting that the accumulation of CCL2-loaded NCs within the tumor site

might represent a valuable strategy to restore the impaired balance of native vs. nitrated/nitrosylated CCL2, in order to rescue CTL recruitment.
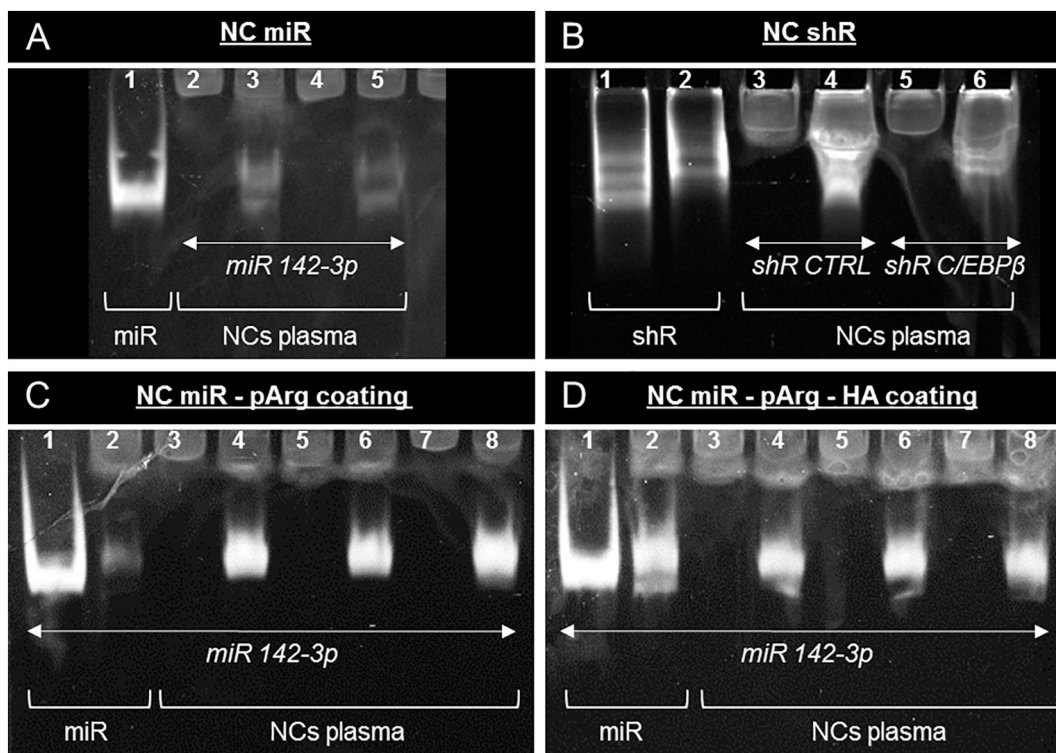
Fig. 4. Release and degradation of RNA from RNAi-loaded NCs after 4 h of incubation in human plasma is controlled by NC engineering with single and multiple polymeric layers and by using RNase resistant sequences. Non-coated NCs (A, B), polyarginine coated NCs (C) and hyaluronic acid-polyarginine coated NCs (D) were diluted 1/10 in human plasma. After 4 h incubation, samples were loaded in 15% polyacrylamide gels with a theoretical RNA amount of 800 ng per well. NC miR lanes: (1) miR- 142-3p sequence in solution; (2) and (4) NCs miR 142-3p incubated in plasma; (3) and (5) NCs miR 142-3p incubated with heparin (30 min on ice). NC shR lanes: (1) and (2) shRNA control (shCTRL) and shC/EBPβ sequences in solution, (3) and (5) NCs shCTRL and NCs shC/EBPβ incubated in plasma, (4) and (6) NCs shCTRL and NCs shC/EBPβ incubated with heparin. NC miR-pArg coating lanes: (1) miR 142-3p sequence in solution; (2) miR 142-3p incubated 30 min with heparin and plasma on ice; (3), (5) and (7) NCs miR 142-3p incubated in plasma; (4), (6) an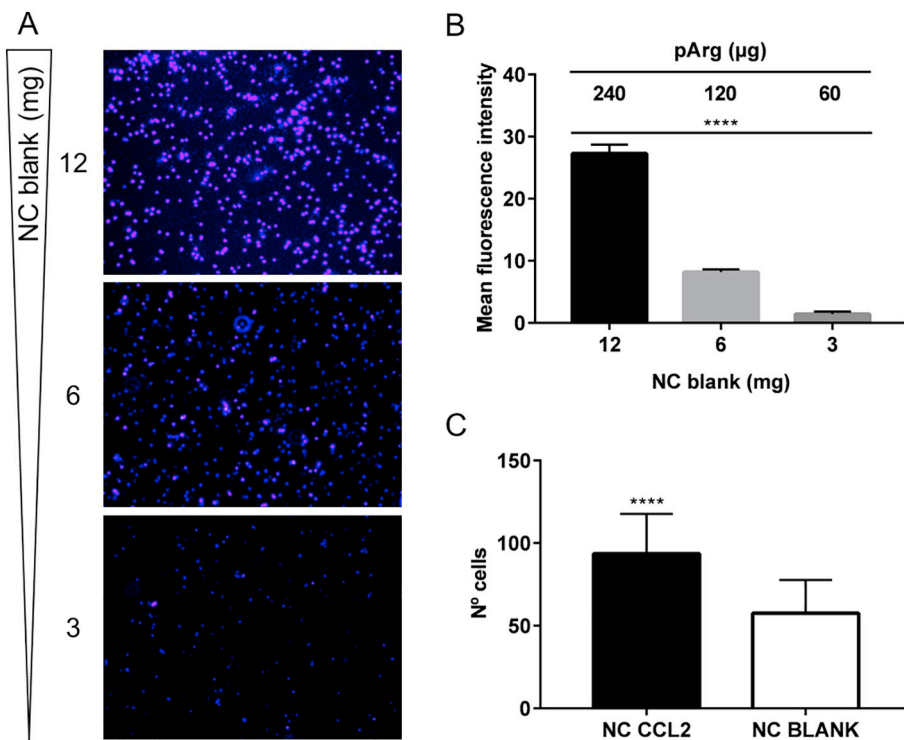d (8) NCs miR 142-3p incubated with heparin. NC miR-pArg-HA coating lanes: (1) miR 142-3p sequence in solution; (2) miR 142-3p incubated 30 min with heparin and plasma on ice; (3), (5) and (7) NCs miR 142-3p incubated in plasma; (4), (6) and (8) NCs miR 142-3p incubated with heparin.

Fig. 5. RAW264.7 macrophages migrate towards pArg NCs in a dose-dependent manner, and this migration is increased by encapsulating CCL2. Transwell assays were performed with blank and CCL2-loaded NCs, and cells that migrated to the basal side of the membrane were DAPI-stained and counted. A) Migration of RAW264.7 macrophages towards decreasing concentrations of blank NCs. Scale bar = 100 μm for all the images. B) Mean fluorescence intensity quantification of (A). C) Macrophage migration to CCL2-loaded NCs as compared to blank NCs. Values represent the mean ± SD of three independent experiments. Data were analyzed using a one-way ANOVA (B) and a two-tailed *t*-Student test (C) (**** $P \leq .0001$).

3.3.2. Effect of miR 142-3p-loaded nanocapsules on BM-MDSC phenotype

It has been shown that in bone marrow (BM)-MDSC cultures, miR-142-3p overexpression prevents the formation of the macrophage fraction (CD11b$^+$Gr-1$^{low-neg}$), which is endowed with the strongest immunosuppressive activity [5]. Consequently, one of the objectives of this study was to investigate the capacity of polyarginine NCs to deliver miR 142-3p and modulate BM-MDSCs.

In a first step, the ability of NCs to facilitate the uptake of RNAi by macrophages was evaluated using a fluorescent RNAi and the RAW264.7 macrophage cell line. A 5′-fluorescein-conjugated miR 142-3p was associated to polyarginine NCs and incubated with the macrophages for 2 h. Free RNAi was also incubated with the macrophages as a control. According to the confocal images shown in Fig. S12, non-coated polyarginine NCs were able to promote RNAi internalization, whereas no detectable signal was observed with free RNAi. Subsequently, the effect of blank polyarginine NCs on MDSC viability and subset cell distribution was studied. The results indicated that polyarginine NCs were highly biocompatible, preserving an adequate cell viability even at a concentration of 100 μg/mL (Fig. S13, Supporting Information), and neglected the contribution of blank NCs on the modulation of MDSCs phenotype (Fig. 6A).

In a second step, the immunomodulatory activity of miR 142-3p-loaded NCs was evaluated. MDSCs were transfected with 0.01–0.2 nmol of miR 142-3p using a commercial transfection reagent (GeneSilencer®, Genlantis) or polyarginine NCs, and percentages of the different cell subsets were quantified by flow cytometry. A scramble miRNA sequence was also loaded in the NCs as control. As depicted in Fig. 6B, miR 142-3p complexed to GeneSilencer® promoted a dramatic reduction of the Gr-1$^{low/negative}$ fraction at the lowest dose of 0.01 nmol. In the case of miR 142-3p-loaded NCs, a dose of around 0.02 nmol was required to exert the same response. For NCs loaded with miR control, the highest dose of 0.2 nmol produced a high reduction on the Gr-1$^{low/negative}$ subset and, consequently, a dose of 0.1 nmol of encapsulated miR 142-3p was selected for further experiments. Representative flow cytometry plots corresponding to transfections performed with the 0.1 nmol dose are depicted in Fig. 6C, visually reflecting the switch towards the Gr-1^{high} phenotype after miR 142-3p treatment. Overall, these results demonstrate the activity of miR 142-3p after NC freeze-drying as well as NCs transfection efficiency and capacity to modulate MDSCs.

3.3.3. In vitro transfection efficiency and in vivo efficacy of C/EBPβ-loaded nanocapsules

As described in the Introduction, C/EBPβ creates a feedback loop with miR-142-3p promoting myeloid cell differentiation towards immunosuppressive macrophages during tumor-induced myelopoiesis [5]. Consequently, C/EBPβ downregulation represents a promising approach to control the immunosuppressive environment and revert tumor-induced tolerance. We thus explored the use of shRNA-loaded polyarginine NCs as a means to silence C/EBPβ in MDSCs. To this end, the transfection efficiency of shC/EBPβ-loaded NCs was first evaluated in MSC-1 cells, an immortalized cell line derived from primary MDSCs [51], using Lipofectamine® RNAiMAX as positive control. shC/EBPβ was titrated from 2.5 to 12.5 pmol/cm^2 to find the optimal dose (maximum silencing with minimum non-specific silencing by control sequences), and a dose of 7.5 pmol/cm^2 was used for the comparative experiments. The shC/EBPβ-loaded NCs caused a significant downregulation of C/EBPβ mRNA compared to either untreated cells or cells treated with NCs and a scrambled sequence. This effect was comparable to the one achieved with the positive control Lipofectamine® RNAiMAX, highlighting the potential of polyarginine NCs for gene delivery and MDSC modulation (Fig. 7A).

Finally, the in vivo efficacy of shC/EBPβ-loaded NCs was assessed in a mouse tumor model. The MCA-203 sarcoma was selected because of the relevant C/EBPβ expression in both tumor infiltrating and splenic myeloid cells, as previously reported [50]. Mice bearing established MCA-203 tumors were intravenously injected with NC-shC/EBPβ or unloaded NCs. Treatments were started at day 11 from tumor injection when tumor surfaces were approximately 35 mm^2, and repeated 3 times with 48 h intervals (RNA dose = 20 μg/mouse/treatment, Fig. 7B). Animals were sacrified 48 h after the last treatment, and CD11b$^+$ myeloid cells were isolated from spleens and tumors by immunomagnetic sorting. C/EBPβ mRNA levels were significantly reduced in both splenic and tumor-infiltrating CD11b$^+$ cells in mice treated with NC-shC/EBPβ compared to controls (Fig. 7C), suggesting the adequate biodistribution of polyarginine NCs to spleen and tumor (Fig. S12, Supporting information). C/EBPβ downregulation was around 50% in splenic myeloid cells and 30% in tumor-infiltrating myeloid cells. No evident signs of toxicity were observed during the treatment period.

To study the impact of C/EBPβ downregulation on tumor-associated myelopoiesis, we performed a phenotypic analysis of myeloid cell subsets in lymphoid organs (spleen and bone marrow) and at the tumor site. While our analysis revealed no differences in bone marrow and splenic myeloid populations (data not shown), a significant decrease in the frequency of tumor-associated macrophages was observed in the NC-shC/EBPβ group compared to controls (Fig. 7D). Such macrophage reduction correlated with a significant increase in monocytic cells (phenotypically definable as M-MDSCs), thus suggesting that C/EBPβ downregulation by RNAi might result in a partial impairment of monocyte differentiation into tumor-associated macrophages.

4. Discussion

The success of adoptive T cell therapy (ACT) for cancer treatment was emphasized by the approval of two Chimeric Antigen Receptor (CAR) T-cell therapies by the Food and Drug Administration (FDA) in 2017 [59]. However, this success is somehow shadowed by the fact that these therapies require prior immune-depleting preparative treatments, which are associated with severe toxicities [60,61]. In this regard, researchers have identified MDSCs as a key immune cell population promoting T cell immunosuppression, and MDSC depletion and RNAi-based re-education have recently proved to be good strategies to improve ACT efficacy [6,32]. In addition, MDSC targeting has proved to benefit other forms of immunotherapy such as vaccination [62,63] and checkpoint blockade therapy [64,65].

The therapeutic efficacy of RNAi-based therapies in vivo may be compromised if they are not integrated in a suitable carrier capable of enhancing their biological half-life and deliver them to their target cell subset. Indeed, the majority of the RNAi therapies under clinical trials rely on the use of a delivery platform [66]. Our proposal assumed that we can re-educate MDSCs by interfering with the C/EBPβ pathway through the use of an RNAi-loaded nanocarrier. Specifically, with this nanocarrier we aim to target the most immunosuppressive monocyte-macrophage MDSCs [5] by the co-encapsulation of the chemokine CCL2, a potent chemoattractant of monocyte-macrophages [8,14,15]. To this end, we developed a nanocapsular system where a GMO lipid core is used to encapsulate CCL2 while the RNAi sequences targeting the C/EBPβ pathway are adsorbed onto a cationic polyarginine shell. By providing CCL2 release within the tumor site, these nanocarriers may also help restore MDSC-impaired CTL recruitment by increasing native CCL2 levels over tumor-nitrated/nitrosylated species [16,18,19].

We selected a GMO lipid core for CCL2 encapsulation due to the favorable structure of GMO-based mesophases for the incorporation and slow release of protein drugs [39,40]. GMO-based mesophases, in particular cubic phases [52], have been explored for protein encapsulation, however, the methods used for their formulation as nanocarriers often require harmful conditions that may damage the drug payload [55,67]. To avoid this, in this study, we developed a new mild self-emulsification method, which involves the use of the non-ionic surfactant Labrasol® to disperse a GMO cubic gel loaded with the protein, yielding polyarginine nanocapsules (NCs). In order to select the

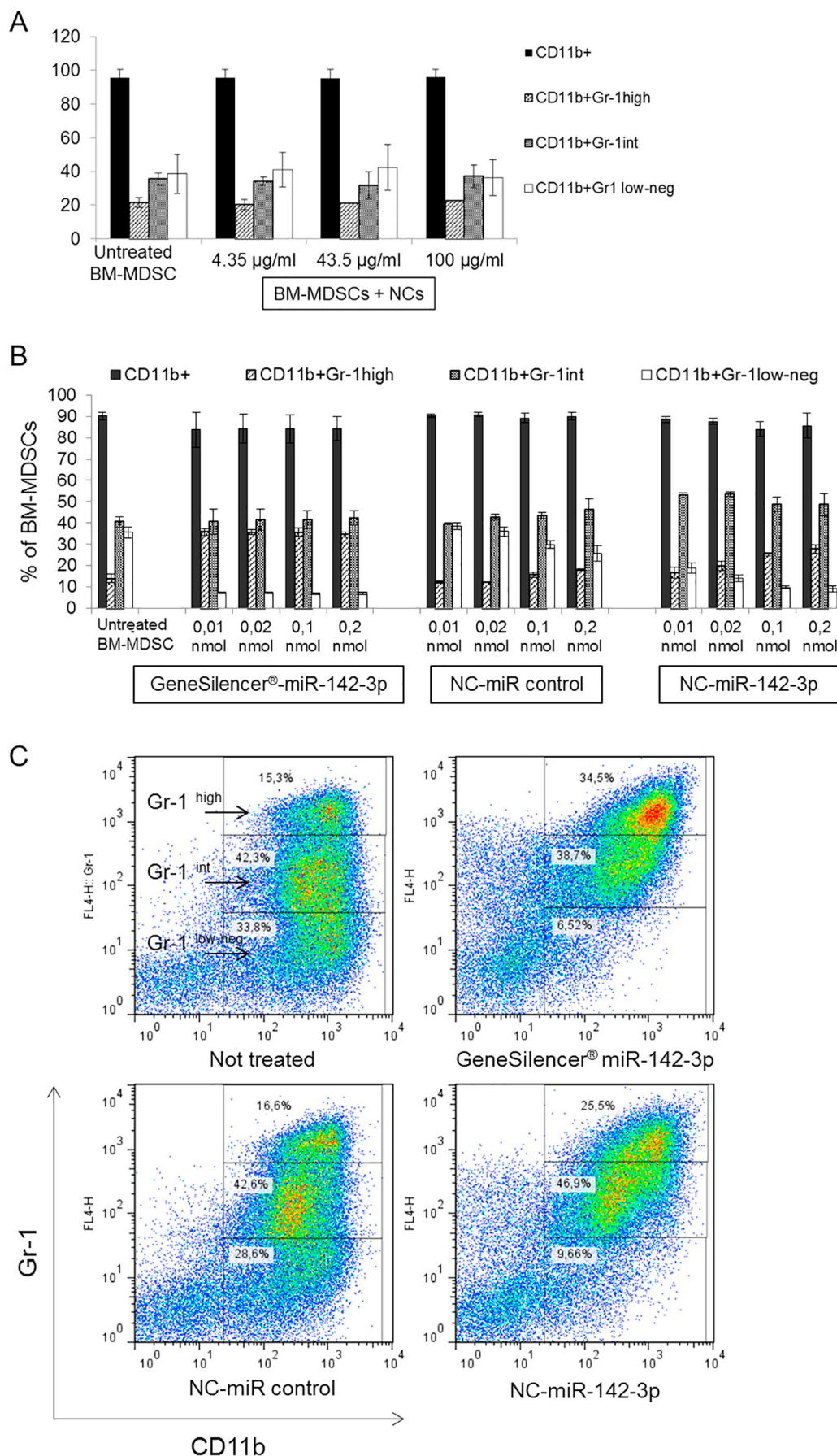**Fig. 6.** Polyarginine NCs loaded with miR-142-3p reduce the percentage of Gr-1$^{low-negative}$ cells (monocyte-macrophage fraction) in primary BM-MDSC cultures. A) MDSCs were treated with increasing concentrations of blank polyarginine NCs to test their effect on subset cell distribution. MDSCs were then transfected with 0.01 to 0.1 nmol of miR 142-3p using a commercial transfection reagent (GeneSilencer®, Genlantis) or polyarginine NCs. The effect of the different doses of miR on bone marrow subsets (B) and representative flow cytometry images for the 0.1 nmol RNA dose (C) are shown. The effects were compared with those seen in cells treated with NCs and a scrambled miR sequence. Values are means ± SD of two independent experiments.
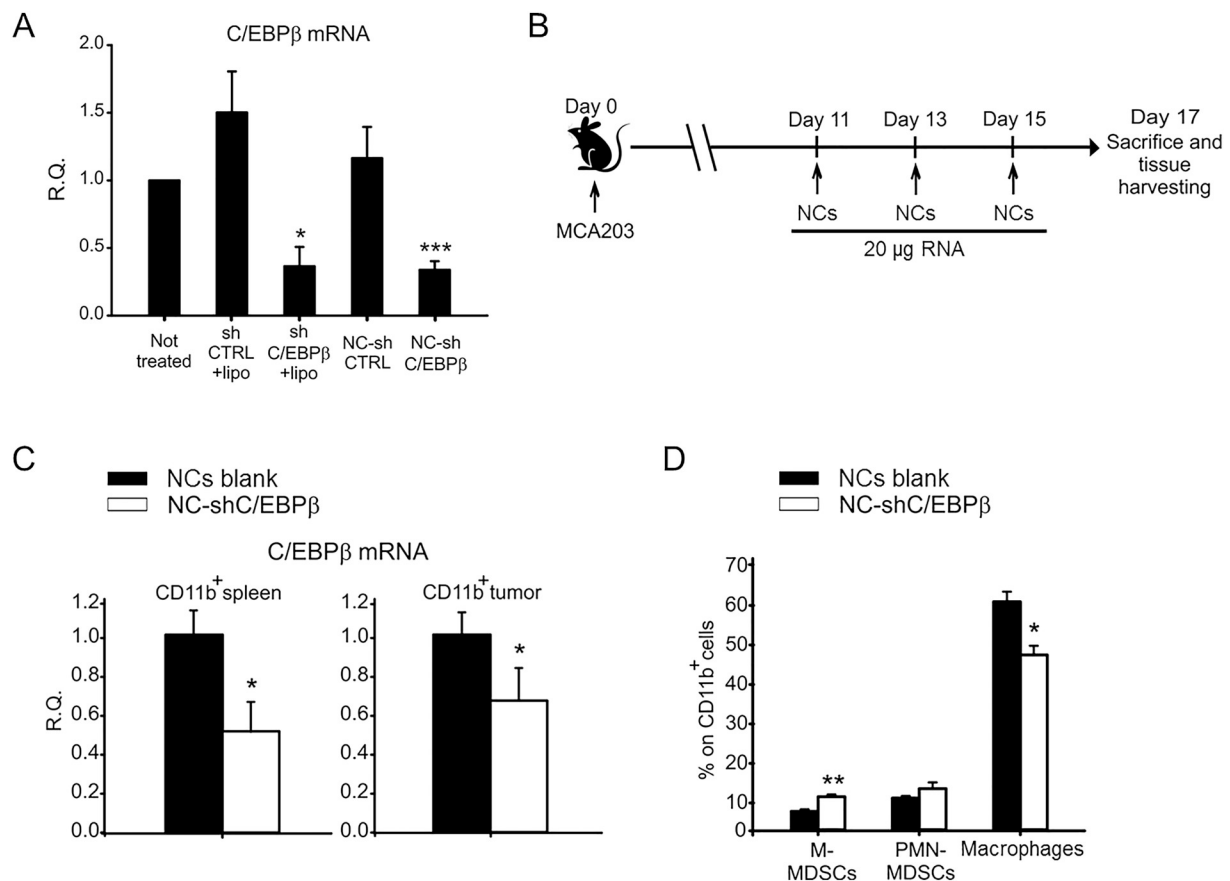
Fig. 7. Polyarginine NCs loaded with C/EBPβ-targeted shRNA downregulate C/EBPβ expression in vitro and in vivo. A) Transfection assay in MSC-1 cells with the modified shRNA. MSC-1 cells were transfected with the C/EBPβ-targeted shRNA (shC/EBPβ) or a scrambled shRNA (shCTRL) either loaded on polyarginine NCs (NC-shC/EBPβ) or complexed with Lipofectamine® RNAiMAX reagent (Invitrogen), and harvested 24 h later. C/EBPβ mRNA levels were quantified by qRT-PCR and normalized with respect to an endogenous control (Rn18S). Data are expressed as relative quantification (R.Q.), normalized to non-transfected (not treated) cells. Means ± SD ($n = 3$). Statistical comparison between each group and the untreated control, *$p \leq .05$, ***$p \leq .001$, Student's *t*-test. B) Schematic representation of the treatment schedule for the in vivo efficacy assay. C57BL/6 mice bearing MCA-203 subcutaneous tumors received three intravenous injections of polyarginine NCs, either blank or loaded with C/EBPβ-targeted shRNA (20 μg RNA/mouse/treatment). Mice were sacrificed 48 h after the last treatment. C) C/EBPβ mRNA levels within CD11b⁺ cells isolated from spleens and tumors of mice treated with either blank NCs, or NCs loaded with the C/EBPβ-targeted shRNA (NC-shC/EBPβ). C/EBPβ mRNA levels were quantified by qRT-PCR and normalized to an endogenous control (Rn18S). Data (means ± SE) are expressed as relative quantification (R.Q.) normalized to the average cycle threshold value for the control group receiving blank NCs. D) Percentage of M-MDSCs, PMN-MDSC and macrophages on total CD11b⁺ cells within the tumor (means ± SD). Cell populations were defined according to the gating strategy reported in Fig. S13. $n = 4$ mice (NC blank) and n = 3 mice (NC-shC/EBPβ). *p ≤ .05, **p ≤ .01, Student's *t*-test.

adequate amount of Labrasol® to disperse this cubic gel, we constructed the phase diagram of the GMO-Labrasol®-water ternary system and evaluated the impact of GMO:Labrasol® w:w ratios on the physico-chemical properties of the nanocarriers. As expected, the addition of increasing amounts of Labrasol® to disperse the cubic gel led to a change from cubic (10% Labrasol®) to inverse micellar (> 20% Labrasol®) phase arrangements. In addition, in order to obtain mono-disperse nanometric particles with adequate colloidal stability over time it was necessary to use a GMO:Labrasol® w:w ratio of 1:9. This composition was selected to prepare CCL2-loaded NCs, achieving adequate protein encapsulation efficiencies of 50% within the L2 inverse micellar phases. This significant encapsulation achieved thanks to the formation of L2 inverse micellar phases represent a relevant result as such phases have been recently reported to provide improved protein release profiles compared to traditionally explored cubic phases [54].

Polyarginine NCs were successfully loaded with two RNAi sequences showing an encapsulation efficiency of 70%, and maintaining their initial physicochemical properties (sizes about 200 nm and PDIs close to 0.1). When these NCs were loaded with miR 142-3p, they were able to modulate MDSCs, switching their most aggressive monocyte-macrophage fraction towards the less immunosuppressive Gr-1ʰⁱᵍʰ

subset, thus confirming the potential of polyarginine NCs as a delivery system for RNAi-based immunomodulation. On their side, shC/EBPβ-loaded NCs promoted a downregulation of C/EBPβ mRNA of 50% and 30% in splenic and tumor-infiltrating myeloid cells, respectively. More importantly, this C/EBPβ downregulation translated into a decrease in the frequency of tumor-associated macrophages (TAMs) and a significant increase in monocytes, pointing to a partial impairment of monocyte differentiation into TAMs. Together, these results suggest that the C/EBPβ-targeted RNAi-loaded NCs are able to modulate the tumor immune infiltrate and could be used to pave the way for enhanced function of complementary cancer immunotherapies.

miR 142-3p and shC/EBPβ were previously reported to enhance the efficacy of ACT and antitumoral DNA vaccination in vivo, respectively, when administered loaded in 4PD dendrimers [6]. Compared to dendrimers, polyarginine NCs may represent more versatile systems for the delivery of drug combinations, a feature that is increasingly demanded in drug delivery, especially in the treatment of complex disease-contexts such as tumor-mediated immunosuppression [68,69]. Indeed, our results show that the encapsulation of the highest dose of CCL2 (1 μg/mL) did not impede the adsorption of miR 142-3p molecules, confirming the suitability of this nanocapsular system for synergistic drug

combinations. In this regard, CCL2-loaded NCs induced a potent chemotactic activity in RAW264.7 macrophages, probing the potential of this co-delivery strategy to target the RNAi therapy to the most immunosuppressive monocyte-macrophage MDSCs. Of note, blank poly-arginine NCs were able to promote a potent macrophage chemoattraction per se, highlighting the potential of these vehicles for cancer immunotherapy and vaccination. Finally, additional functionalities can be added to the NCs surface following previously explored layer-by-layer approaches [70–73]. This strategy could be used to modulate the interaction of the NCs and the cell milieu, to increase the number of encapsulated drugs or to protect them. For this last purpose, RNA-loaded NCs were assembled with multiple polymer layers creating a "sandwich-like" organization that preserved miR 142-3p integrity during at least 4 h of incubation in human plasma.

The results presented here show a significant silencing of C/EBPβ mRNA within spleen and tumor after in vivo administration of shC/EBPβ-loaded NCs, and a potent migration of macrophages and T cells towards CCL2 in vitro. Further studies would be needed to investigate whether CCL2-loaded NCs are able to revert T cell anergy and preferentially target the most immunosuppressive MDSCs subsets as compared to blank NCs. However, given the passive tumor targeting capacity of nanocarriers [35], and the Matrigel®-invasion capacity of Jurkat T cells towards a CCL2 gradient, we anticipate that CCL2-loaded NCs could represent a valuable strategy to restore native CCL2 levels within the tumor site and rescue cytotoxic lymphocyte recruitment. Altogether, these observations already show that the combination of the chemoattractive properties of the polyarginine NCs and the C/EBPβ-targeted RNAi is enough to drive the modulation of the tumor immunosuppressive environment, potentially providing a therapeutic benefit.

5. Conclusions

A new mild self-emulsifying method was developed to generate polyarginine nanocapsules (NCs) that enabled the *co*-encapsulation of chemokines and polynucleotides. The method was based on the dispersion of a GMO cubic gel, which resulted in the formation of L2 inverse micellar phases adequate for the entrapment of hydrophilic payloads (i.e. CCL2). In addition, the polyarginine shell facilitated the attachment of RNAi molecules, which were then protected with additional single polyarginine or double polyarginine/HA polymer layers. When loaded with miR 142-3p, these NCs enabled RNAi transfection in MDSCs, and promoted the reversion of their highly immunosuppressive phenotype. More importantly, NCs loaded with shC/EBPβ were able to reduce C/EBPβ mRNA levels within the spleen and tumor of a mouse fibrosarcoma model, reducing monocyte differentiation into tumor-associated macrophages. Finally, these NCs provide a controlled delivery of CCL2, and were able to promote a high degree of macrophage migration towards the particles. Overall, the observations presented herein suggest that polyarginine NCs represent a promising carrier for the co-delivery of RNAi and chemokines, which may help modulate the activity of MDSCs.

Acknowledgements

Appendix A. Supplementary data

Supplementary data to this article can be found online at https://doi.org/10.1016/j.jconrel.2018.12.041.

References

[1] A. Sica, V. Bronte, J. Clin. Invest. 117 (2007) 1155.
[2] F. De Sanctis, S. Solito, S. Ugel, B. Molon, V. Bronte, I. Marigo, Biochim. Biophys. Acta Rev. Cancer 1865 (2016) 35.
[3] A. Arina, V. Bronte, Curr. Opin. Immunol. 33 (2015) 120.
[4] F. Torres Andón, M.J. Alonso, J. Drug Target. 23 (2015) 656.
[5] N. Sonda, F. Simonato, E. Peranzoni, B. Calì, S. Bortoluzzi, A. Bisognin, E. Wang, F.M. Marincola, L. Naldini, B. Gentner, C. Trautwein, S.D. Sackett, P. Zanovello, B. Molon, V. Bronte, Immunity 38 (2013) 1236.
[6] S. Zilio, J.L. Vella, A.C. De la Fuente, P.M. Daftarian, D.T. Weed, A. Kaifer, I. Marigo, K. Leone, V. Bronte, P. Serafini, J. Immunol. 198 (2017) 4166.
[7] A. Viola, A. Sarukhan, V. Bronte, B. Molon, Trends Immunol. 33 (2012) 496.
[8] B.-Z. Qian, J. Li, H. Zhang, T. Kitamura, J. Zhang, L.R. Campion, E.A. Kaiser, L.A. Snyder, J.W. Pollard, Nature 475 (2011) 222.
[9] R.D. Loberg, C. Ying, M. Craig, L. Yan, L.A. Snyder, K.J. Pienta, Neoplasia 9 (2007) 556.
[10] A.L. Chang, J. Miska, D.A. Wainwright, M. Dey, C.V. Rivetta, D. Yu, D. Kanojia, K.C. Pituch, J. Qiao, P. Pytel, Y. Han, M. Wu, L. Zhang, C.M. Horbinski, A.U. Ahmed, M.S. Lesniak, Cancer Res. 76 (2016) 5671.
[11] E. Chun, S. Lavoie, M. Michaud, C.A. Gallini, J. Kim, G. Soucy, R. Odze, J.N. Glickman, S. Wendy, Cell Rep. 12 (2015) 244.
[12] M. Hale, F. Itani, C.M. Buchta, G. Wald, M. Bing, L.A. Norian, PLoS One 10 (2015) 1.
[13] B. Huang, Z. Lei, J. Zhao, W. Gong, J. Liu, Z. Chen, Y. Liu, D. Li, Y. Yuan, G.M. Zhang, Z.H. Feng, Cancer Lett. 252 (2007) 86.
[14] W. Bin Fang, M. Yao, G. Brummer, D. Acevedo, N. Alhakamy, C. Berkland, N. Cheng, W. Bin Fang, M. Yao, G. Brummer, D. Acevedo, N. Alhakamy, C. Berkland, N. Cheng, W. Bin Fang, M. Yao, G. Brummer, D. Acevedo, N. Alhakamy, C. Berkland, N. Cheng, Oncotarget 7 (2014) 49349.
[15] Y. Sawanobori, S. Ueha, Blood 111 (2008) 5457.
[16] A.M. Lesokhin, T.M. Hohl, S. Kitano, C. Cortez, D. Hirschhorn-Cymerman, F. Avogadri, G.A. Rizzuto, J.J. Lazarus, E.G. Pamer, A.N. Houghton, T. Merghoub, J.D. Wolchok, Cancer Res. 72 (2012) 876.
[17] S.A. Rosenberg, M.E. Dudley, Proc. Natl. Acad. Sci. U. S. A. 101 (Suppl) (2004) 14639.
[18] B. Molon, S. Ugel, F. Del Pozzo, C. Soldani, S. Zilio, D. Avella, A. De Palma, P. Mauri, A. Monegal, M. Rescigno, B. Savino, P. Colombo, N. Jonjic, S. Pecanic, L. Lazzarato, R. Fruttero, A. Gasco, V. Bronte, A. Viola, J. Exp. Med. 208 (2011) 1949.
[19] B. Molon, A. Viola, V. Bronte, Oncoimmunology 1 (2012) 390.
[20] N. Nagarsheth, M.S. Wicha, W. Zou, Nat. Rev. Immunol. (2017), https://doi.org/10.1038/nri.2017.49.
[21] S.A. Bencherif, R.W. Sands, O.A. Ali, W.A. Li, S.A. Lewin, T.M. Braschlera, T.-Y.S. Shih, C.S. Verbeke, D. Bhatta, G. Dranofff, D.J. Mooney, Nat. Commun. 6 (2016) 7556.
[22] J. Kim, W.A. Li, Y. Choi, S.A. Lewin, C.S. Verbeke, G. Dranoff, D.J. Mooney, Nat. Biotechnol. 33 (2014) 64.
[23] O.A. Ali, P. Tayalia, D. Shvartsman, S. Lewin, D.J. Mooney, Adv. Funct. Mater. 23 (2013) 4621.
[24] J. Shi, P.W. Kantoff, R. Wooster, O.C. Farokhzad, Nat. Rev. Cancer 17 (2016) 20.
[25] S.B. Sondike, E.M. Pisetsky, J.L. Luzier, J. Immunol. 196 (2016) 2167.
[26] X. Tian, J. Tian, X. Tang, K. Rui, Y. Zhang, J. Ma, Y. Wang, H. Xu, L. Lu, S. Wang, Oncoimmunology 4 (2015) 1.
[27] M.È. Lebel, K. Chartrand, E. Tarrab, P. Savard, D. Leclerc, A. Lamarre, Nano Lett. 16 (2016) 1826.
[28] A. Fernandez, C. Mesa, I. Marigo, L. Dolcetti, M. Clavell, L. Oliver, L.E. Fernandez, V. Bronte, J. Immunol. 186 (2011) 264.
[29] D. Sun, X. Zhuang, X. Xiang, Y. Liu, S. Zhang, C. Liu, S. Barnes, W. Grizzle, D. Miller, H.-G. Zhang, Mol. Ther. 18 (2010) 1606.
[30] Y. Zhao, S.C. Burkert, Y. Tang, D.C. Sorescu, A.A. Kapralov, G.V. Shurin, M.R. Shurin, V.E. Kagan, A. Star, J. Am. Chem. Soc. 137 (2015) 675.
[31] L. Jeanbart, I.C. Kourtis, A.J. van der Vlies, M.A. Swartz, J.A. Hubbell, Cancer Immunol. Immunother. 64 (2015) 1033.
[32] M.S. Sasso, G. Lollo, M. Pitorre, S. Solito, L. Pinton, S. Valpione, G. Bastiat, S. Mandruzzato, V. Bronte, I. Marigo, J.P. Benoit, Biomaterials 96 (2016) 47.
[33] F. Torres, E. Digi, A. Maeda, M. Erreni, A. Mantovani, M. José, P. Allavena, Semin. Immunol. 34 (2017) 103.
[34] V. Bronte, S. Brandau, S.-H. Chen, M.P. Colombo, A.B. Frey, T.F. Greten, S. Mandruzzato, P.J. Murray, A. Ochoa, S. Ostrand-Rosenberg, P.C. Rodriguez, A. Sica, V. Umansky, R.H. Vonderheide, D.I. Gabrilovich, Nat. Commun. 7 (2016) 12150.
[35] Y. Nakamura, A. Mochida, P.L. Choyke, H. Kobayashi, Bioconjug. Chem. 27 (2016) 2225.
[36] M.P. Kai, H.E. Brighton, C.A. Fromen, T.W. Shen, J.C. Luft, Y.E. Luft, A.W. Keeler, G.R. Robbins, J.P.Y. Ting, W.C. Zamboni, J.E. Bear, J.M. DeSimone, ACS Nano 10 (2016) 861.

[37] D.I. Gabrilovich, S. Ostrand-Rosenberg, V. Bronte, Nat. Rev. Immunol. 12 (2012) 253.

[38] V. Bronte, M.J. Pittet, Immunity (2013) *39*, 806.

[39] C.J. Drummond, C. Fong, Curr. Opin. Colloid Interface Sci. 4 (1999) 449.

[40] J. Clogston, M. Caffrey, J. Control. Release 107 (2005) 97.

[41] F.K. Szabo, G.E. Hoffman, Biomaterials 32 (2011) 5717.

[42] M.V. Lozano, G. Lollo, M. Alonso-Nocelo, J. Brea, A. Vidal, D. Torres, M.J. Alonso, J. Nanopart. Res. 15 (2013) 1515.

[43] S. Reimondez-Troitiño, I. Alcalde, N. Csaba, A. Íñigo-Portugués, M. de la Fuente, F. Bech, A.C. Riestra, J. Merayo-Lloves, M.J. Alonso, Drug Deliv. Transl. Res. 6 (2016) 708.

[44] G. Lollo, A. Gonzalez-Paredes, M. Garcia-Fuentes, P. Calvo, D. Torres, M.J. Alonso, J. Pharm. Sci. 106 (2017) 611.

[45] Z. Niu, E. Tedesco, F. Benetti, A. Mabondzo, I.M. Montagner, I. Marigo, D. Gonzalez-Touceda, S. Tovar, C. Dieguez, M.J. Santander-Ortega, M.J. Alonso, J. Control. Release 263 (2017) 4.

[46] A. Gonzalez-paredes, D. Torres, M.J. Alonso, Int. J. Pharm. 529 (2017) 474.

[47] N.M. Kirby, S.T. Mudie, A.M. Hawley, D.J. Cookson, H.D.T. Mertens, N. Cowieson, V. Samardzic-Boban, J. Appl. Crystallogr. 46 (2013) 1670.

[48] S.T. Hyde, Handb. Appl. Surf. Colloid Chem. (2001) 299.

[49] C.A. Schneider, W.S. Rasband, K.W. Eliceiri, Nat. Methods 9 (2012) 671.

[50] I. Marigo, E. Bosio, S. Solito, C. Mesa, A. Fernandez, L. Dolcetti, S. Ugel, N. Sonda, S. Bicciato, E. Falisi, F. Calabrese, G. Basso, P. Zanovello, E. Cozzi, S. Mandruzzato, V. Bronte, Immunity 32 (2010) 790.

[51] E. Apolloni, V. Bronte, A. Mazzoni, P. Serafini, A. Cabrelle, D.M. Segal, H.A. Young, P. Zanovello, J. Immunol. 165 (2000) 6723.

[52] H. Qiu, M. Ca, Biomaterials 21 (2000) 223.

[53] J. Zhai, L. Waddington, T.J. Wooster, M.I. Aguilar, B.J. Boyd, Langmuir 27 (2011) 14757.

[54] S. Phan, W.K. Fong, N. Kirby, T. Hanley, B.J. Boyd, Int. J. Pharm. (2011) *421*, 176.

[55] D.P. Chang, M. Jankunec, J. Barauskas, F. Tiberg, T. Nylander, Langmuir 28 (2012) 10688.

[56] S. Rizwan, T. Hanley, B. Boyd, T. Rades, S. Hook, J. Pharm. Sci. 98 (2009) 4191.

[57] Y. Yang, J. Wolfram, X. Fang, H. Shen, M. Ferrari, Small 10 (2014) 1250.

[58] M.C. Maa, M.Y. Chang, J. Li, Y.Y. Li, M.Y. Hsieh, C.J. Yang, Y.J. Chen, Y. Li, H.C. Chen, W.E. Cheng, C.Y. Hsieh, C.W. Cheng, T.H. Leu, Biochim. Biophys. Acta Mol. Cell Res. 1813 (2011) 136.

[59] P. Zheng, J.M. Kros, J. Li, Drug Discov. Today (2018) 00, https://doi.org/10.1016/j.drudis.2018.02.012.

[60] S.A. Rosenberg, J.C. Yang, R.M. Sherry, U.S. Kammula, S. Marybeth, G.Q. Phan, D.E. Citrin, N.P. Restifo, P.F. Robbins, R. John, K.E. Morton, C.M. Laurencot, S.M. Steinberg, E. Donald, M.E. Dudley, Clin. Cancer Res. 17 (2011) 4550.

[61] M.J. Besser, R. Shapira-Frommer, O. Itzhaki, A.J. Treves, D.B. Zippel, D. Levy, A. Kubi, N. Shoshani, D. Zikich, Y. Ohayon, D. Ohayon, B. Shalmon, G. Markel, R. Yerushalmi, S. Apter, A. Ben-Nun, E. Ben-Ami, A. Shimoni, A. Nagler, J. Schachter, Clin. Cancer Res. 19 (2013) 4792.

[62] C. De Santo, P. Serafini, I. Marigo, L. Dolcetti, M. Bolla, P. Del Soldato, C. Melani, C. Guiducci, M.P. Colombo, M. Iezzi, P. Musiani, P. Zanovello, V. Bronte, Proc. Natl. Acad. Sci. U. S. A. 102 (2005) 4185.

[63] A. Bose, J.L. Taylor, S. Alber, S.C. Watkins, J.A. Garcia, B.I. Rini, J.S. Ko, P.A. Cohen, J.H. Finke, W. J. Storkus 129 (2011) 2158.

[64] S.L. Highfill, Y. Cui, A.J. Giles, J.P. Smith, H. Zhang, E. Morse, R.N. Kaplan, C.L. Mackall, Sci. Transl. Med. 6 (2014) 237.

[65] R. Zappasodi, T. Merghoub, J.D. Wolchok, Cancer Cell 33 (2018) 581.

[66] R. Rupaimoole, F.J. Slack, Nat. Rev. Drug Discov. 16 (2017) 203.

[67] J. Barauskas, M. Johnsson, F. Joabsson, F. Tiberg, Langmuir 21 (2005) 2569.

[68] R.X. Zhang, J. Li, T. Zhang, M.A. Amini, C. He, B. Lu, T. Ahmed, H. Lip, A.M. Rauth, X.Y. Wu, Acta Pharmacol. Sin. 39 (2018) 825.

[69] R.X. Zhang, H.L. Wong, H.Y. Xue, J.Y. Eoh, X.Y. Wu, J. Control. Release 240 (2016) 489.

[70] Y.F. Tan, R.C. Mundargi, M.H.A. Chen, J. Lessig, B. Neu, S.S. Venkatraman, T.T. Wong, Small 10 (2014) 1790.

[71] A. Elbakry, E.C. Wurster, A. Zaky, R. Liebl, E. Schindler, P. Bauer-Kreisel, T. Blunk, R. Rachel, A. Goepferich, M. Breunig, Small 8 (2012) 3847.

[72] Z. Chen, L. Zhang, Y. He, Y. Shen, Y. Li, Small 11 (2015) 952.

[73] A. Elbakry, A. Zaky, R. Liebl, R. Rachel, A. Goepferich, M. Breunig, Nano Lett. 9 (2009) 2059.